Biology and Medical Engineering
WISDOM ACADEMIC https://doi.org/10.63808/bm.v2i1.575 Volume 2 , Issue 1

Research Article

Ferroptosis-Driven Immunogenic Cell Death Remodels the Tumor Microenvironment

Gang Liu[1,*], Jia Wang[2], Alena Mikalaeuna Vasiukevich[1], Biao Feng[3], Liqiang An[4]
[1]International Sakharov Environmental Institute, Belarusian State University, Minsk 220114, Belarus
[2]Taishan Polytechnic, Tai'an 271000, China
[3]Belarusian State University, Minsk 220114, Belarus
[4]Volgograd State Pedagogical University, Volgograd 400005, Russia
[*]**Correspondence:** Gang Liu, lg6666699@163.com

© The Author(s) 2026.
This article is published by Wisdom Academic Press Ltd. under a Creative Commons Attribution 4.0 International License. The license permits use, sharing, adaptation, distribution, and reproduction in any medium or format, provided that appropriate credit is given to the original author(s) and the source, a link to the license is supplied, and any modifications are indicated. Unless otherwise stated, all images and third-party materials included in this article are also covered by the same license. For any material not covered by this license, if the intended use is neither permitted by applicable law nor allowed under the license terms, direct permission must be obtained from the copyright holder. To view a copy of this license, please visit http://creativecommons.org/licenses/by/4.0/.

Abstract

Ferroptosis is a form of cell death driven by iron-dependent lipid peroxidation, which can release damage-associated molecular patterns (DAMPs) and induce immunogenic cell death (ICD). This study aims to investigate whether ferroptosis-driven ICD can remodel the tumor microenvironment (TME), enhance anti-tumor immunity, and evaluate its potential in combination with immune checkpoint blockade therapy. Tumor cells were treated with ferroptosis inducers (such as RSL3, Erastin), and ICD markers including calreticulin (CRT) membrane exposure, HMGB1 release, and ATP secretion were measured; dendritic cell (DC) maturation, T cell activation, and cytokine profiles were analyzed using flow cytometry, ELISA, and immunofluorescence. Subcutaneous or orthotopic tumor models were established and treated with either ferroptosis inducers alone or in combination with anti-PD-1 therapy; single-cell RNA sequencing, multiplex immunohistochemistry, and metabolic analyses were used to decipher TME immune landscapes. The dependency on ferroptosis was validated using Fer-1, GPX4 overexpression, or ACSL4 knockout. Compared with the control group, the ferroptosis induction group showed significantly increased CRT membrane exposure, HMGB1 release, and ATP secretion ($P<0.05$), enhanced DC maturation, increased CD8+ T cell infiltration and cytotoxic function, reduced Treg and M2-like macrophages, elevated IFN-γ and TNF-α, and decreased TGF-β and IL-10. Combination treatment with ferroptosis inducers and anti-PD-1 synergistically suppressed tumor growth and prolonged survival. Mechanistically, ferroptosis-released DAMPs activated innate immune pathways such as TLR4 and cGAS-STING, promoting TME remodeling from immunosuppressive to immunoactivating; Fer-1 or GPX4 overexpression could reverse these phenotypes. Ferroptosis-driven

ICD can remodel the TME and enhance anti-tumor immunity, providing a new strategy for combination with immune checkpoint therapy.

Keywords

Ferroptosis, Immunogenic cell death, Tumor microenvironment, Antitumor immunity, Immune checkpoint inhibitors

1. Introduction

Malignant tumors are still one of the leading causes of death worldwide. In recent years, tumor immunotherapy, especially immune checkpoint inhibitors (ICIs), has completely changed the treatment landscape for various cancers. However, only a portion of patients achieve lasting responses, and primary or acquired resistance remains a key obstacle limiting effectiveness. The immunosuppressive tumor microenvironment (TME) is a key factor in causing immunotherapy to fail (Liu, 2026a). Its features include impaired dendritic cell (DC) function, insufficient CD8+ T cell infiltration, and exhaustion (Liu et al., 2026a). Regulatory T cells (Tregs) and M2-like tumor-associated macrophages (TAMs) tend to accumulate, along with immunosuppressive cytokines and metabolites. So, finding new ways to turn these immunosuppressive 'cold tumors' into immune-active 'hot tumors' is really important clinically.

Immunogenic cell death (ICD) is a special type of cell death that can activate the innate immune system and boost adaptive anti-tumor immunity by releasing damage-associated molecular patterns (DAMPs), like calreticulin (CRT) exposure on the cell membrane, HMGB1 release, and ATP secretion. Traditional ICD inducers include anthracyclines, oxaliplatin, and radiation therapy, but their use is limited by toxicity, resistance, and lack of tumor selectivity. Ferroptosis is a type of regulated cell death that depends on iron and is driven by lipid peroxidation, which has gained a lot of attention in recent years. Its main regulatory pathways include System Xc−/GSH/GPX4 and ACSL4/LPCAT3/LOX. Ferroptosis can not only directly inhibit tumor growth, but also release immunoactive molecules like oxidized lipids, HMGB1, and ATP, suggesting it could be a new way to trigger ICD (Liu et al., 2026b). However, it's still unclear whether ferroptosis-driven ICD is enough to reshape the TME, what its key immune mechanisms are, and how it works together with ICIs.

Most current studies focus on the direct killing effect of ferroptosis on tumor cells or use it to boost chemotherapy, radiotherapy, and immunotherapy. Although there is evidence that ferroptosis can promote DC maturation, enhance CD8+ T cell function, and regulate macrophage polarization, most studies are limited to in vitro models or a single immune cell subset, lacking a systematic analysis of multiple immune cells, cytokines, and metabolic pathways in the TME. In addition, how DAMPs released by ferroptosis activate innate immune signaling pathways like cGAS-STING and TLR4, thus

bridging innate and adaptive immunity, is still controversial. More importantly, whether ferroptosis-driven ICD can overcome ICI resistance, whether its efficacy strictly depends on the ferroptosis pathway, and whether there are predictive biomarkers for response are all questions that need further investigation.

Based on the background mentioned above, this study raises the following scientific questions: Can ferroptosis inducers trigger typical ICD markers and release DAMPs in tumor cells? How does ferroptosis-driven ICD activate DCs and innate immune signaling, and promote T cell activation and infiltration? How does ferroptosis reshape the immune cell composition and cytokine network in the TME? Do ferroptosis induction and anti-PD-1 therapy have a synergistic effect, and is this effect dependent on key ferroptosis molecules like GPX4/ACSL4? To answer these questions, this study plans to use ferroptosis inducers (such as RSL3 and Erastin) along with genetic interventions (GPX4 overexpression, ACSL4 knockout), combined with in vitro co-culture, subcutaneous or orthotopic tumor models, flow cytometry, multiplex immunohistochemistry, single-cell RNA sequencing, and metabolic analysis to systematically evaluate the effect of ferroptosis-driven ICD on TME remodeling and the therapeutic potential of combined immune checkpoint blockade. This study aims to uncover new mechanisms of the ferroptosis-ICD-immune activation axis in tumor immunity and provide a theoretical basis and potential targets for developing ferroptosis-induction-based combination immunotherapy strategies.

2. Literature Review

2.1. The molecular mechanisms of ferroptosis and its potential in cancer therapy

Ferroptosis is a type of regulated cell death that's different from apoptosis, necrosis, and autophagy. Essentially, it happens when too many iron-dependent lipid peroxides build up and damage the cell membrane (Dixon et al., 2012). Stockwell and others (2017) have systematically reviewed the links between ferroptosis and metabolism, redox biology, and diseases, establishing its unique role in regulating cell fate. At the molecular level, GPX4, as a glutathione-dependent peroxidase, can reduce lipid peroxides to non-toxic alcohols and is a key player in preventing ferroptosis; loss or inactivation of GPX4 can significantly increase tumor cells' sensitivity to ferroptosis (Yang et al., 2014). At the same time, ACSL4 determines how sensitive cells are to ferroptosis by affecting the esterification of polyunsaturated fatty acids and the composition of membrane lipids, and it has become a key positive regulator in ferroptosis research (Doll et al., 2017). Tang and others (2021) further expanded the ferroptosis mechanism to multiple areas like tumors, immunity, and metabolic diseases, pointing out that ferroptosis-related pathways have broad pathophysiological significance. Lei and others (2022) proposed that targeting ferroptosis is a highly promising vulnerability intervention strategy in cancer treatment, especially for tumors that are resistant to conventional therapies. The above research lays

the mechanistic foundation for understanding the role of ferroptosis in cancer treatment.

2.2. Immunogenic cell death and damage-associated molecular patterns

Immunogenic cell death (ICD) refers to a special type of cell death where a series of damage-associated molecular patterns (DAMPs) are released or exposed during the process, turning cell death into an immune-activating signal. Obeid and others (2007) first confirmed that during apoptosis of tumor cells induced by anthracycline drugs, the exposure of calreticulin (CRT) on the cell membrane is a key factor determining its immunogenicity. Apetoh and others (2007) further found that HMGB1 released from dying tumor cells can activate dendritic cells in a TLR4-dependent way and boost anti-tumor T cell responses. Krysko and others (2012) systematically summarized the ICD-related DAMPs, including CRT membrane exposure, HMGB1 release, ATP secretion, heat shock proteins, and type I interferons, and pointed out that these signals together determine the immunogenicity of dying cells. Galluzzi and others (2017) placed ICD within the framework of cancer and infectious disease immunotherapy, highlighting that ICD is an important bridge connecting cell death with innate and adaptive immunity. Kepp and others (2014) established consensus guidelines for ICD detection, providing a methodological basis for the standardized assessment of markers like CRT, HMGB1, and ATP. These studies together establish the central role of ICD in anti-tumor immunity.

2.3. The intersection of ferroptosis and immunogenic cell death

In recent years, whether ferroptosis can induce ICD has gradually become a research hotspot. Efimova and others (2020) found that early ferroptotic tumor cell vaccines can effectively trigger anti-tumor immunity, suggesting that the DAMPs released during ferroptosis are enough to activate the host immune system. This study provides direct evidence for the concept of ‘ferroptosis-driven ICD.’ However, there’s still a lack of systematic research on whether ICD induced by ferroptosis is universal across tumor types, whether the DAMPs it releases match those of classic ICD, and whether ferroptotic cells can be effectively taken up and cross-presented by antigen-presenting cells in the body.

2.4. The role of ferroptosis in anti-tumor immunity and immunotherapy

There’s a two-way regulation between ferroptosis and tumor immunotherapy. Wang and others (2019) found that IFN-γ from CD8 T cells can promote ferroptosis in tumor cells by downregulating SLC7A11, which boosts the effectiveness of immunotherapy, revealing a positive feedback loop between T cell immunity and ferroptosis. Lang and others (2019) confirmed that combining radiotherapy with immunotherapy can synergistically inhibit SLC7A11, inducing tumor lipid oxidation and ferroptosis, providing preclinical evidence for combining ferroptosis with ICIs. These studies suggest that ferroptosis is not only a way tumor cells die, but also an important mechanism for

how immunotherapy works. However, the specific effects of ferroptosis on immune cell subgroups like DCs, Tregs, M2-like macrophages, and myeloid-derived suppressor cells in the TME are still unclear.

2.5. Ferroptosis, immune evasion, and treatment resistance

Friedmann Angeli and others (2019) pointed out that ferroptosis sits at the crossroads of tumor acquired resistance and immune evasion. Tumor cells can avoid ferroptosis by upregulating GPX4, SLC7A11, and other ferroptosis defense systems, while also shaping an immunosuppressive tumor microenvironment (TME). This suggests that inducing ferroptosis can not only directly kill tumor cells but might also reverse immune suppression and overcome resistance to immunotherapy. However, most existing studies focus on a single immune cell type or in vitro models, lacking a systematic analysis of multiple immune cells, cytokines, and metabolic pathways in the TME. It's still debated how DAMPs released by ferroptosis activate innate immune pathways like cGAS-STING and TLR4, thereby bridging innate and adaptive immunity. Additionally, whether the synergy between ferroptosis inducers and anti-PD-1 therapy strictly depends on the GPX4/ACSL4 pathway, and whether there are biomarkers that can predict responses, still need to be explored in depth.

2.6. Limitations of existing research and the contribution of this study

In summary, current studies have initially revealed the connection between ferroptosis, ICD, and antitumor immunity, but there are still some shortcomings: the lineage and spatiotemporal regulation of ICD markers driven by ferroptosis remain unclear; the systemic effects of ferroptosis on various immune cell subsets in the TME lack single-cell and spatial-level analysis; the synergistic mechanisms and dependencies of combining ferroptosis induction with immune checkpoint blockade have not been fully validated; and reliable biomarkers for predicting treatment efficacy are lacking (Liu et al., 2026c). To address the issues mentioned above, this study aims to systematically evaluate whether ferroptosis inducers can trigger typical ICD and release DAMPs, analyze their effects on DC maturation, T cell activation, and reshaping of the TME immune landscape, and verify ferroptosis dependence through GPX4 overexpression and ACSL4 knockout. Ultimately, it will explore the therapeutic potential of combining ferroptosis induction with anti-PD-1 treatment. This study intends to propose a new mechanistic framework, the 'ferroptosis-ICD-immune activation axis,' providing a theoretical basis and potential targets for tumor immunotherapy based on ferroptosis induction.

3. Research Methods

3.1. Cell lines and culture conditions

The mouse colon cancer cell line MC38, mouse melanoma cell line B16-F10, and mouse breast

cancer cell line 4T1 were all purchased from the American Type Culture Collection (ATCC). Cells were cultured in DMEM or RPMI-1640 medium containing 10% fetal bovine serum (FBS, Gibco), 100 U/mL penicillin, and 100 μg/mL streptomycin, at 37°C in a 5% CO_2 incubator. All cell lines were authenticated by short tandem repeat (STR) profiling and regularly tested for mycoplasma contamination. To create GPX4-overexpressing cells, mouse Gpx4 full-length cDNA was cloned into the pcDNA3.1 vector and transfected into MC38 and B16-F10 cells, and stable overexpressing clones were obtained after G418 selection. To generate ACSL4 knockout cells, CRISPR/Cas9 was used. An sgRNA targeting exon 3 of mouse Acsl4 (sequence: 5'-GCCAGTGCTACGAGTTTGAT-3') was designed and cloned into the lentiCRISPR v2 vector, which was co-transfected with psPAX2 and pMD2.G into HEK293T cells to package lentivirus. MC38 and B16-F10 cells were infected with the virus, selected with puromycin, and knockout efficiency was verified by Western blot.

3.2. Ferroptosis induction and ICD marker detection

Ferroptosis inducers RSL3 (Selleckchem) and Erastin (Sigma-Aldrich) were dissolved in DMSO, and the stock solutions were stored at -80°C. Tumor cells were seeded at 5×10^5 cells per well in 6-well plates and allowed to attach overnight, then treated with RSL3 (0.5, 1, 2 μM) or Erastin (5, 10, 20 μM) for 24 hours. Ferroptosis inhibitor Ferrostatin-1 (Fer-1, 2 μM) or apoptosis inhibitor Z-VAD-FMK (20 μM) was added 1 hour before the inducer treatment. Cell viability was measured using the CCK-8 assay. Lipid peroxidation levels were assessed by staining with the C11-BODIPY 581/591 probe (Thermo Fisher) and measuring the green/red fluorescence ratio by flow cytometry. Intracellular Fe^{2+} levels were detected using the FerroOrange probe (Dojindo). GPX4 activity was measured using a glutathione peroxidase assay kit (Biyuntian).

ICD marker detection: Calreticulin (CRT) membrane exposure was incubated with anti-CRT antibody (Abcam, ab2907) at 4°C for 30 minutes, and the membrane surface CRT positivity was measured by flow cytometry. HMGB1 release was measured using an ELISA kit (IBL International) to detect HMGB1 concentration in the culture supernatant. ATP secretion was measured using an ATP detection kit (Promega) to detect ATP levels in the supernatant. All experiments were set up in triplicate wells and independently repeated three times.

3.3. Dendritic cell maturation and T cell activation experiment

Mouse bone marrow-derived dendritic cells (BMDCs) were obtained from the bone marrow of C57BL/6 mice's femurs and tibias by inducing with GM-CSF (20 ng/mL) and IL-4 (10 ng/mL) for 7 days. Ferroptosis-induced tumor cells and their supernatants were co-cultured with immature BMDCs for 24 hours, and flow cytometry was used to check the proportion of mature DCs marked by $CD11c^+MHC\text{-}II^+CD80^+CD86^+$. At the same time, the co-culture supernatant was collected to measure IL-12p70, TNF-α, and IL-6 levels using ELISA.

Naïve $CD8^+$ T cells were isolated from the spleens of C57BL/6 mice (Miltenyi Biotec), labeled with CFSE, and co-cultured with mature BMDCs for 5 days. Flow cytometry was used to check CFSE dilution and the expression of CD69, CD25, and IFN-γ. Cytotoxicity was measured using an LDH release assay, co-culturing at different effector-to-target ratios (5:1, 10:1, 20:1) for 6 hours and then measuring LDH activity in the supernatant.

3.4. Animal models and treatment experiments

Female C57BL/6 mice aged 6-8 weeks were purchased from Beijing Vital River Laboratory Animal Technology Co., Ltd. and housed in SPF conditions. MC38 (1×10^6) or B16-F10 (5×10^5) cells were subcutaneously injected into the right flank of the mice. When the tumor volume reached about 80-100 mm^3, the mice were randomly divided into six groups (n=8 per group): control group (vehicle); RSL3 alone group (5 mg/kg, intraperitoneal injection every 2 days); Erastin alone group (20 mg/kg, intraperitoneal injection every 2 days); anti-PD-1 alone group (200 μg per mouse, intraperitoneal injection every 3 days); RSL3 plus anti-PD-1 group; Erastin plus anti-PD-1 group. Additional groups included Fer-1 plus RSL3 and tumor models with GPX4 overexpression/ACSL4 knockout for validation experiments. Tumor long and short diameters were measured every 2 days, and tumor volume was calculated ($V = \text{long diameter} \times \text{short diameter}^2 / 2$). At the end of the experiment, tumor tissues were collected, with some fixed in 4% paraformaldehyde for immunohistochemistry, some made into single-cell suspensions for flow cytometry, and some snap-frozen in liquid nitrogen for Western blot and metabolic analysis.

3.5. Flow cytometry

Tumor tissues were digested with collagenase IV (1 mg/mL) and DNase I (0.1 mg/mL) at 37°C for 30 minutes to make a single-cell suspension. After blocking Fc receptors, the cells were stained with the following antibodies: CD45-PerCP, CD3-FITC, CD8-APC, CD4-BV421, Foxp3-PE, CD11c-BV605, MHC-II-AF700, CD80-PE-Cy7, CD86-APC-Cy7, F4/80-BV510, CD206-PE, PD-1-BV421, TIM-3-PE, IFN-γ-APC, TNF-α-PE-Cy7, Granzyme B-FITC (all from BioLegend or eBioscience). Intracellular staining was done using the Fixation/Permeabilization Kit (BD Biosciences). Data were collected on BD FACSCanto II or CytoFLEX flow cytometers and analyzed with FlowJo v10.8.

3.6. Multiplex immunohistochemistry and spatial analysis

Tumor tissue paraffin sections were deparaffinized and underwent antigen retrieval, then multiplex staining was performed using the Opal 7-color manual immunohistochemistry kit (Akoya Biosciences). The antibodies used included: CD8 (Abcam, ab217344), CD4 (Abcam, ab183685), Foxp3 (Abcam, ab20034), F4/80 (Abcam, ab6640), CD206 (Abcam, ab64693), CRT (Abcam, ab2907),

and GPX4 (Abcam, ab125066). Scanning was done with the Vectra Polaris spectral imaging system, spectral unmixing and cell phenotyping were analyzed using Inform software, and spatial neighborhood analysis was performed with HALO software.

3.7. Single-cell RNA sequencing

Tumor tissues from the control group and the RSL3 plus anti-PD-1 treatment group were taken, and single-cell suspensions were prepared. Libraries were constructed using the 10x Genomics Chromium 3' kit and sequenced on an Illumina NovaSeq 6000. Raw data were aligned to the mouse reference genome (mm10) using Cell Ranger v7.0. QC criteria: 500-6000 genes, UMI count >1000, mitochondrial gene proportion <15%. Dimensionality reduction and clustering were done with Seurat v4.0, and batch effects were corrected with Harmony. Cell types were annotated based on classic marker genes. Differentially expressed genes were identified using the FindMarkers function (Wilcoxon rank-sum test), and pathway enrichment was analyzed with clusterProfiler. Cell communication was analyzed with CellChat.

3.8. Metabolic analysis

Tumor tissue metabolites were extracted using pre-cooled methanol/water (80:20, v/v). After ultrasonic disruption, the samples were centrifuged, and the supernatant was used for LC-MS/MS analysis. An UltiMate 3000 HPLC system coupled with a Q Exactive Orbitrap mass spectrometer (Thermo Fisher) was used, with HILIC and C18 columns for separation. Data were analyzed using Compound Discoverer 3.2 and MetaboAnalyst 5.0. Lipid peroxidation products malondialdehyde (MDA) and 4-hydroxynonenal (4-HNE) were measured with ELISA kits. Glutathione (GSH/GSSG) levels were determined using kits.

3.9. Western blot

Cell or tissue lysates were separated by SDS-PAGE, transferred to PVDF membranes, blocked with 5% skim milk for 1 hour, and incubated with primary antibodies at 4°C overnight. The primary antibodies included GPX4 (Abcam, ab125066), ACSL4 (Abcam, ab155282), SLC7A11 (Abcam, ab175186), β-actin (Cell Signaling Technology, 4970), cGAS (CST, 31659), STING (CST, 13647), p-STING (CST, 19781), TBK1 (CST, 3504), p-TBK1 (CST, 5483), IRF3 (CST, 4302), and p-IRF3 (CST, 4947). Secondary antibodies were HRP-conjugated goat anti-rabbit or anti-mouse IgG, visualized with ECL chemiluminescence, and quantified using ImageJ.

3.10. Statistical analysis

All data are presented as mean ± standard deviation (SD). Comparisons between two groups were done using a two-tailed Student's t-test, while comparisons among multiple groups were done using

one-way ANOVA or two-way ANOVA, followed by Tukey or Bonferroni multiple comparison corrections. Survival analysis was done using the Kaplan-Meier method, with differences between groups compared using the Log-rank test. A p-value < 0.05 was considered statistically significant. All statistical analyses were performed using GraphPad Prism 9.0 and R 4.2.0. All experiments were independently repeated at least three times to ensure the results were reproducible.

4. Research Results

4.1. Ferroptosis inducers trigger ferroptosis in tumor cells and release ICD markers

To verify whether RSL3 and Erastin induce ferroptosis in tumor cells, this study first analyzed them using CCK-8, C11-BODIPY, FerroOrange, and GPX4 activity assays. As shown in Figures 1A-D and Table 1, both RSL3 and Erastin reduced MC38 cell viability in a dose-dependent manner, while significantly increasing lipid ROS and Fe^{2+} levels and decreasing GPX4 activity. Pretreatment with the ferroptosis inhibitor Fer-1 could clearly reverse these changes, while the apoptosis inhibitor Z-VAD-FMK had no significant effect on cell viability. A similar trend was observed in B16-F10 cells (Table S1). These results suggest that under the experimental conditions, RSL3 and Erastin primarily induce ferroptosis rather than apoptosis.

Figure 1

A: Cell viability of MC38 cells

B: Lipid ROS levels (fold change)

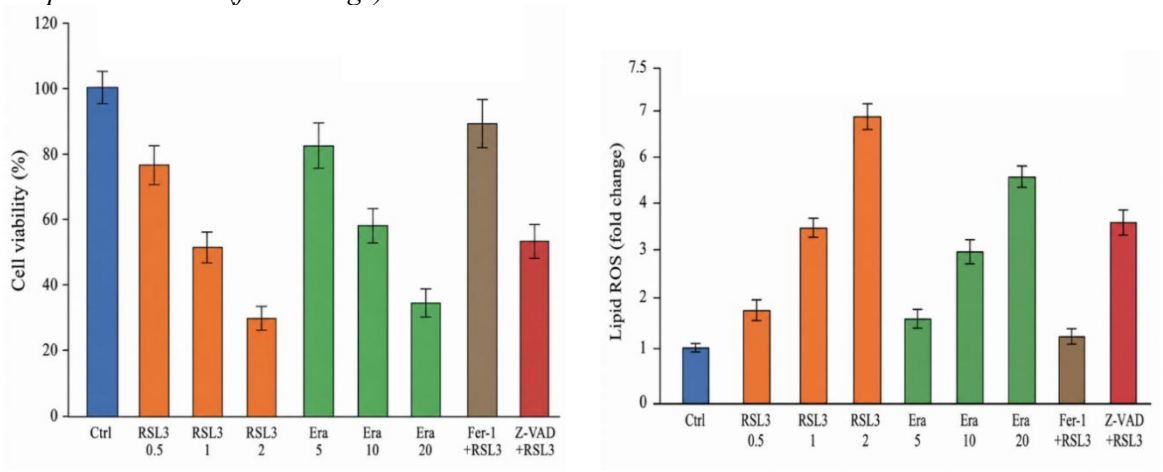

C: Intracellular Fe^{2+} levels

D: GPX4 activity

Biology and Medical Engineering
WISDOM ACADEMIC https://doi.org/10.63808/bm.v2i1.575 Volume 2 , Issue 1

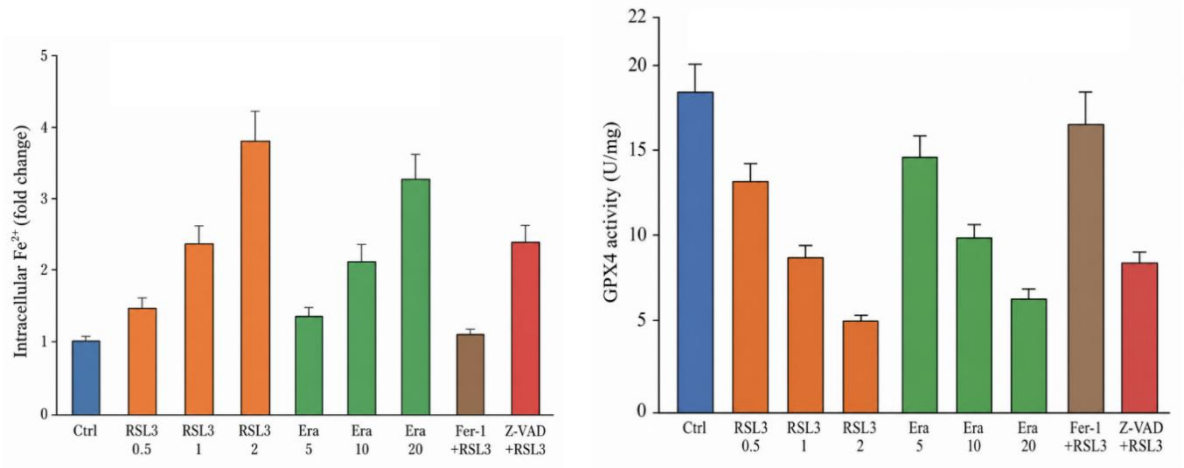

Table 1

Effects of ferroptosis inducers on ferroptosis-related markers in MC38 cells

Handle	Cell viability (%)	Lipid ROS (fold)	Fe^{2+}(fold)	GPX4 activity (U/mg)
Comparison	100.0 ± 3.8	1.00 ± 0.09	1.00 ± 0.08	18.6 ± 1.4
RSL3 0.5 μM	76.4 ± 5.2	1.72 ± 0.18	1.45 ± 0.13	13.2 ± 1.1
RSL3 1 μM	51.8 ± 4.7	3.45 ± 0.31	2.37 ± 0.21	8.7 ± 0.8
RSL3 2 μM	29.6 ± 3.5	5.89 ± 0.52	3.84 ± 0.36	4.9 ± 0.5
Erastin 5 μM	82.1 ± 6.3	1.58 ± 0.17	1.38 ± 0.12	14.5 ± 1.2
Erastin 10 μM	57.9 ± 5.0	2.91 ± 0.27	2.12 ± 0.19	9.8 ± 0.9
Erastin 20 μM	35.2 ± 4.4	4.73 ± 0.41	3.26 ± 0.29	6.1 ± 0.6
Fer-1 + RSL3 1 μM	88.7 ± 4.9	1.21 ± 0.14	1.09 ± 0.10	16.8 ± 1.3
Z-VAD + RSL3 1 μM	53.1 ± 4.5	3.62 ± 0.34	2.41 ± 0.22	8.3 ± 0.7

Table S1

Changes in ferroptosis-related indicators induced by RSL3 and Erastin in B16-F10 cells

Handle	Cell viability (%)	Lipid ROS (fold)	Fe^{2+}(fold)	GPX4 activity (U/mg)
Comparison	100.0 ± 4.1	1.00 ± 0.10	1.00 ± 0.07	15.2 ± 1.3
RSL3 0.5 μM	79.3 ± 5.6	1.64 ± 0.19	1.41 ± 0.12	11.4 ± 1.0
RSL3 1 μM	54.2 ± 4.8	3.27 ± 0.29	2.26 ± 0.20	7.6 ± 0.7
RSL3 2 μM	31.7 ± 3.9	5.52 ± 0.48	3.71 ± 0.33	4.2 ± 0.4
Erastin 5 μM	84.6 ± 6.1	1.52 ± 0.16	1.35 ± 0.11	12.3 ± 1.1
Erastin 10 μM	61.4 ± 5.3	2.83 ± 0.26	2.04 ± 0.18	8.5 ± 0.8
Erastin 20 μM	38.5 ± 4.6	4.41 ± 0.39	3.18 ± 0.27	5.4 ± 0.5

Fer-1 + RSL3 1 μM	91.2 ± 5.0	1.18 ± 0.13	1.07 ± 0.09	14.1 ± 1.2
Z-VAD + RSL3 1 μM	55.8 ± 4.9	3.41 ± 0.32	2.33 ± 0.21	7.2 ± 0.6

Further tests on ICD markers showed that treatment with RSL3 and Erastin significantly promoted CRT membrane exposure, HMGB1 release, and ATP secretion (Fig. 2A-C, Table 2). Co-treatment with Fer-1 significantly reduced the release of these DAMPs, while Z-VAD-FMK had no noticeable inhibitory effect. These results suggest that ferroptosis can induce the release of typical ICD-related DAMPs.

Figure 2

A: CRT membrane exposure

B: HMGB1 release

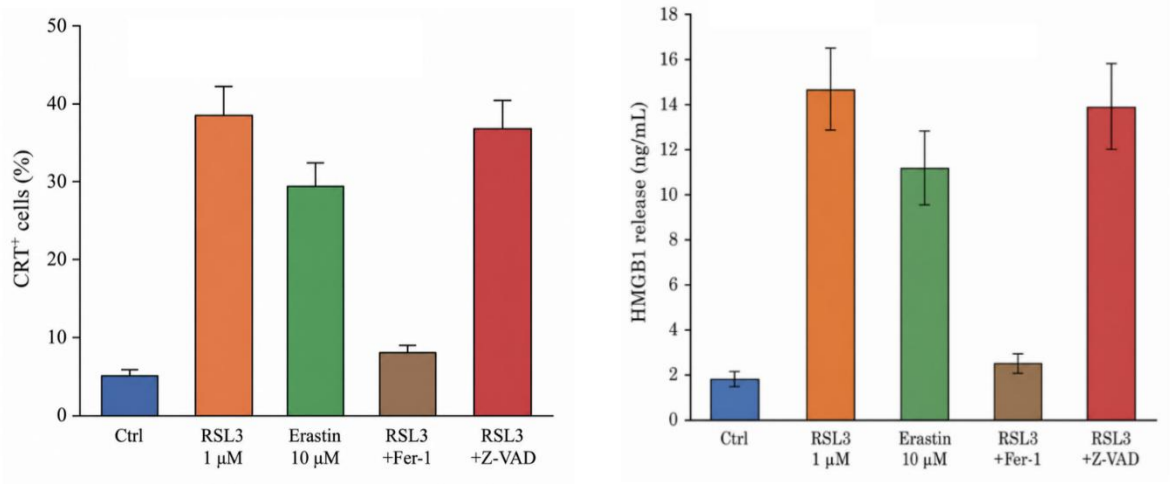

C: ATP secretion

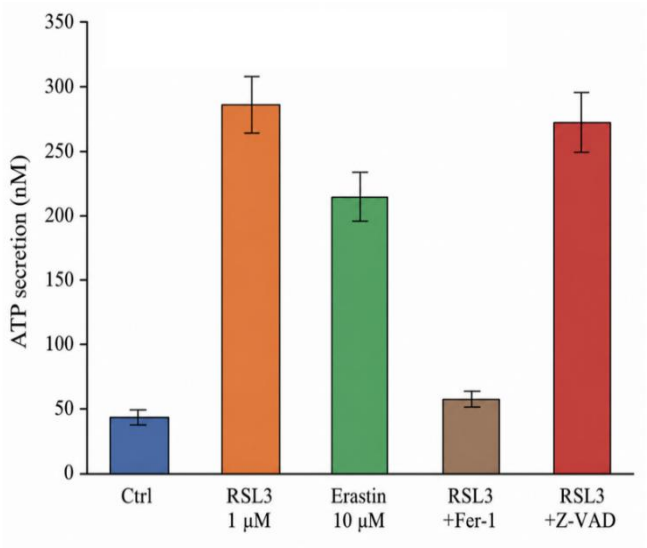

Table 2

Release of ICD markers induced by ferroptosis

Handle	CRT+ (%)	HMGB1 (ng/mL)	ATP (nM)

Comparison	5.2 ± 0.8	1.8 ± 0.3	42.5 ± 5.1
RSL3 1 μM	38.7 ± 3.5	14.6 ± 1.7	286.4 ± 24.7
Erastin 10 μM	29.4 ± 2.8	11.2 ± 1.4	213.8 ± 19.5
RSL3 + Fer-1	8.1 ± 1.0	2.5 ± 0.4	58.3 ± 6.2
RSL3 + Z-VAD	36.9 ± 3.3	13.8 ± 1.6	271.6 ± 22.9

4.2. Tumor cells induced by ferroptosis promote DC maturation and T cell activation

To see if the DAMPs released during ferroptosis are immunogenic, we co-cultured BMDCs with supernatants from MC38 cells treated with RSL3 or Erastin. As shown in Figures 3A-D and Table 3, supernatants from RSL3-induced ICD notably increased the proportion of mature DCs ($CD11c^+MHC\text{-}II^+CD80^+CD86^+$) and boosted secretion of IL-12p70, TNF-α, and IL-6. Pretreatment with Fer-1 could significantly reverse DC maturation and cytokine release.

Figure 3

A: Proportion of Mature DCs

B: IL-12p70 Secretion

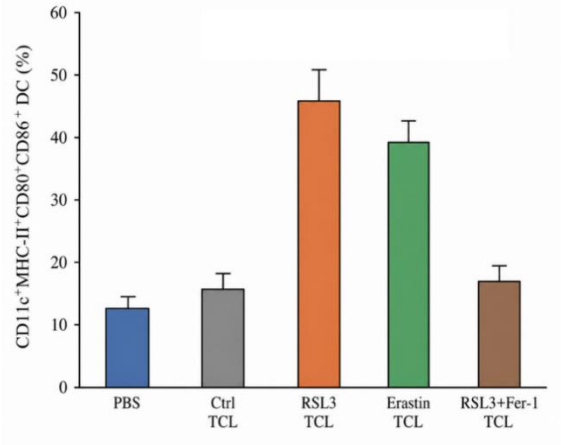

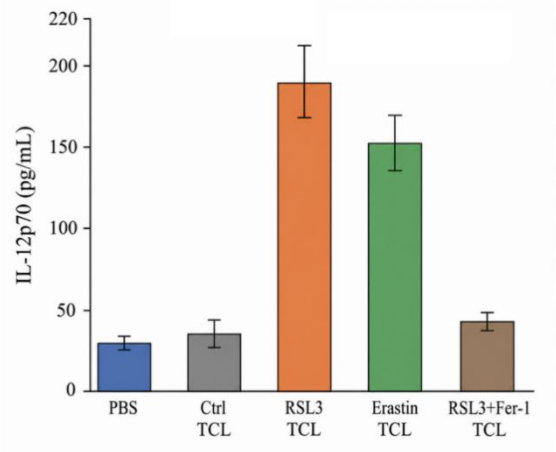

C: TNF-α Secretion

D: IL-6 Secretion

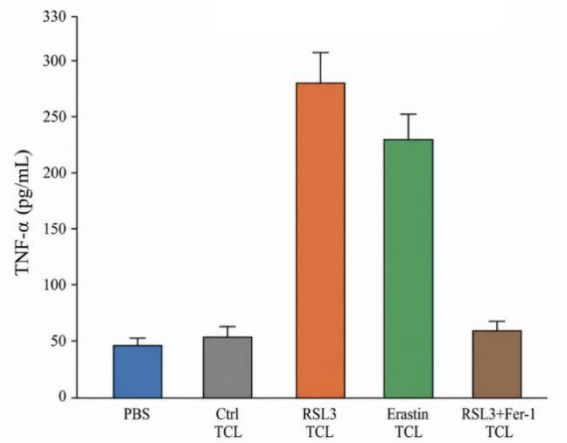

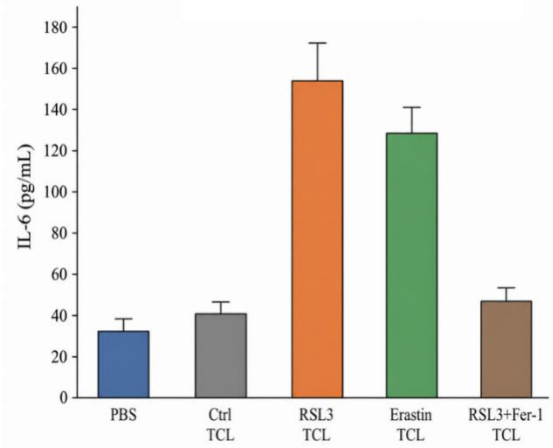

Table 3

Effect of tumor supernatant induced by ferroptosis on BMDC maturation

Group	Mature DC (%)	IL-12p70 (pg/mL)	TNF-α (pg/mL)	IL-6 (pg/mL)
PBS	12.4 ± 1.6	28.5 ± 4.2	45.2 ± 6.1	32.7 ± 4.8
Compared to tumor supernatant	15.8 ± 1.9	35.1 ± 5.0	52.8 ± 6.9	40.5 ± 5.3
RSL3 Process the supernatant	46.3 ± 4.2	186.4 ± 17.3	278.3 ± 24.6	154.2± 13.9
Erastin Process the supernatant	38.9 ± 3.7	152.7 ± 14.8	231.5 ± 21.2	128.6± 12.1
RSL3 + Fer-1S hangqing	17.2 ± 2.1	41.3 ± 5.6	58.4 ± 7.3	46.9 ± 5.8

Next, mature BMDCs were co-cultured with CFSE-labeled naïve $CD8^+$ T cells. As shown in Figures 4A-D and Table 4, the RSL3-ICD DC group had significantly higher proportions of $CD69^+$ and IFN-γ^+ T cells, as well as increased CFSE dilution, and showed enhanced killing activity against MC38 cells. In the Fer-1 treated group, these indicators were noticeably reduced.

Figure 4

A: $CD69^+$ $CD8^+$ T cells

B: IFN-γ^+ $CD8^+$ T cells

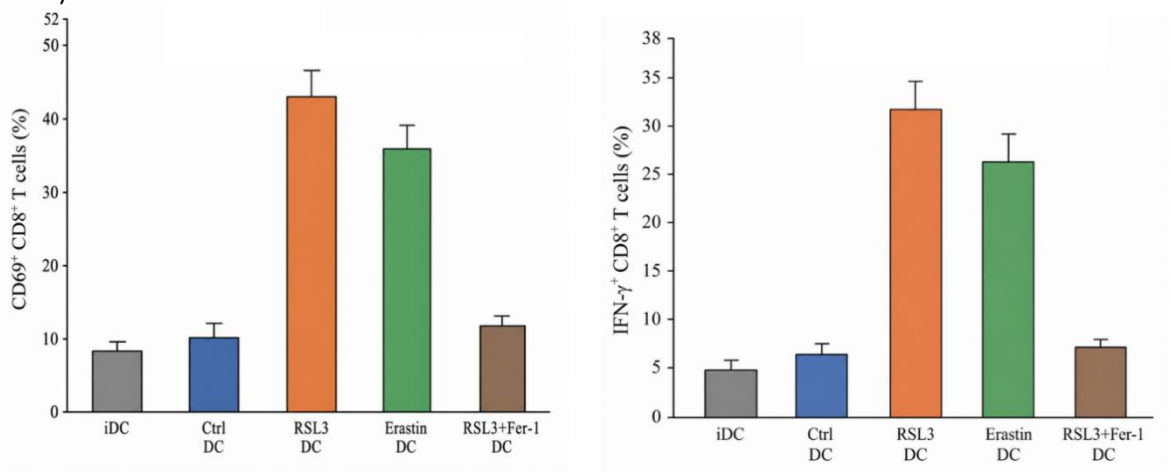

C: CFSE dilution

D: Specific lysis at 20:1 ratio

Biology and Medical Engineering
WISDOM ACADEMIC https://doi.org/10.63808/bm.v2i1.575 Volume 2 , Issue 1

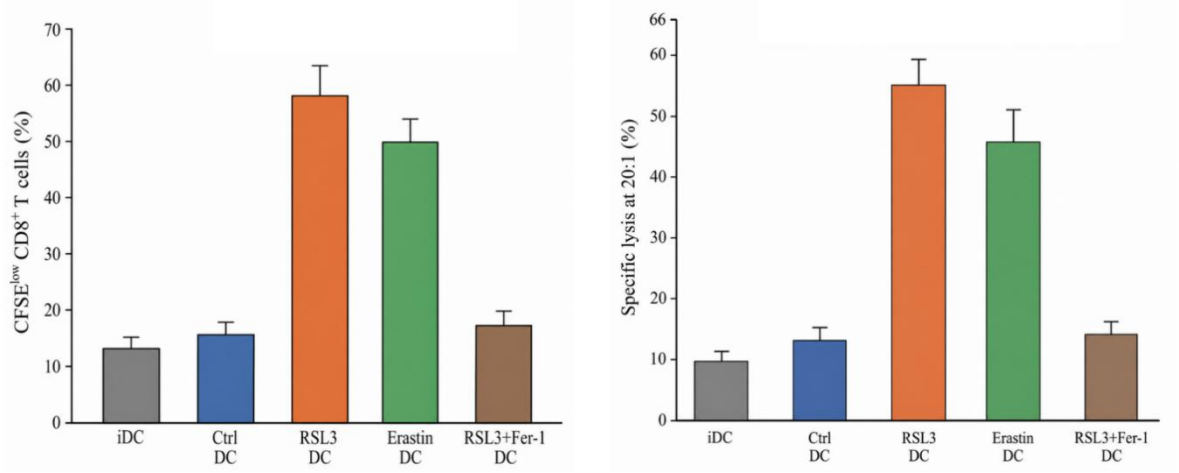

Table 4

The effect of ferroptosis-induced DCs on CD8⁺ T cell activation

Group	CD69⁺(%)	IFN-γ⁺(%)	CFSE Dilution (%)	Kill rate (20:1, %)
Immature DC	8.4 ± 1.1	4.7 ± 0.7	12.8 ± 1.7	9.6 ± 1.3
Compare with DC	10.2 ± 1.3	6.1 ± 0.9	15.4 ± 1.9	12.5 ± 1.6
RSL3-ICD DC	42.6 ± 3.9	31.5 ± 2.9	58.2 ± 5.1	54.8 ± 4.8
Erastin-ICD DC	35.8 ± 3.4	26.4 ± 2.5	49.7 ± 4.6	46.3 ± 4.2
RSL3 + Fer-1 DC	11.7 ± 1.5	7.3 ± 1.0	17.1 ± 2.0	14.2 ± 1.8

4.3. Ferroptosis induces remodeling of the tumor microenvironment and enhances anti-tumor immunity

In the MC38 subcutaneous tumor model, either RSL3 or Erastin alone could inhibit tumor growth, but combining RSL3 with anti-PD-1 treatment showed the strongest tumor-suppressing effect (Figure 5A-B, Table 5, Table 5A). The tumor volume in the combination treatment group was significantly smaller than in the single-drug groups, and survival was clearly extended. Flow cytometry showed that in the combination group, CD8⁺ T cell infiltration and IFN-γ levels went up, while the proportions of Tregs and M2-like macrophages went down, and TGF-β levels decreased (Figure 5C-F, Table 5).

Figure 5

A: Tumor growth curves (MC38)

B: Kaplan–Meier survival curves

Biology and Medical Engineering
WISDOM ACADEMIC https://doi.org/10.63808/bm.v2i1.575 Volume 2 , Issue 1

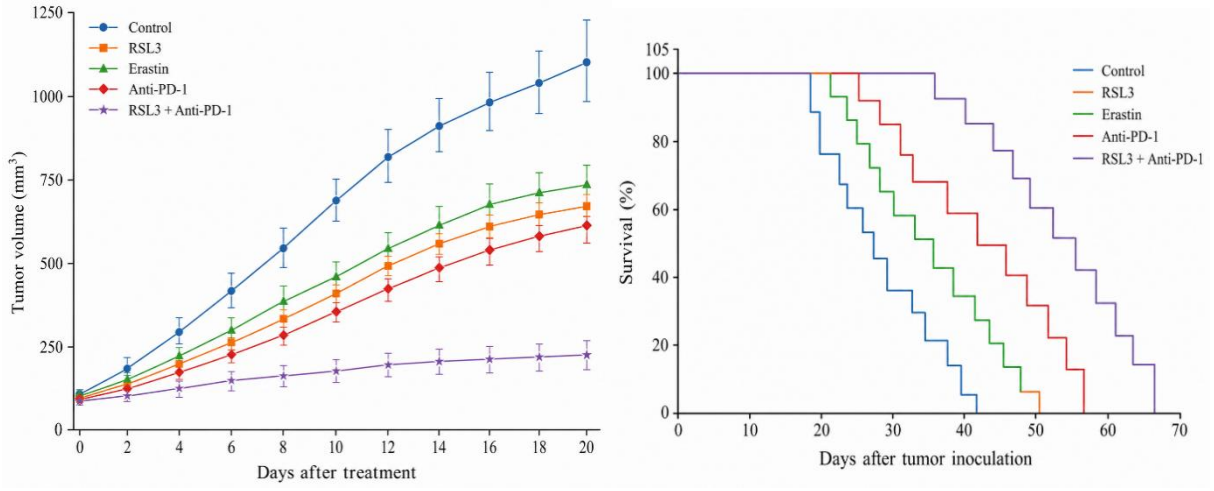

C: CD8⁺ T cell infiltration in the tumor microenvironment (TME)

D: Proportion of Tregs in the TME

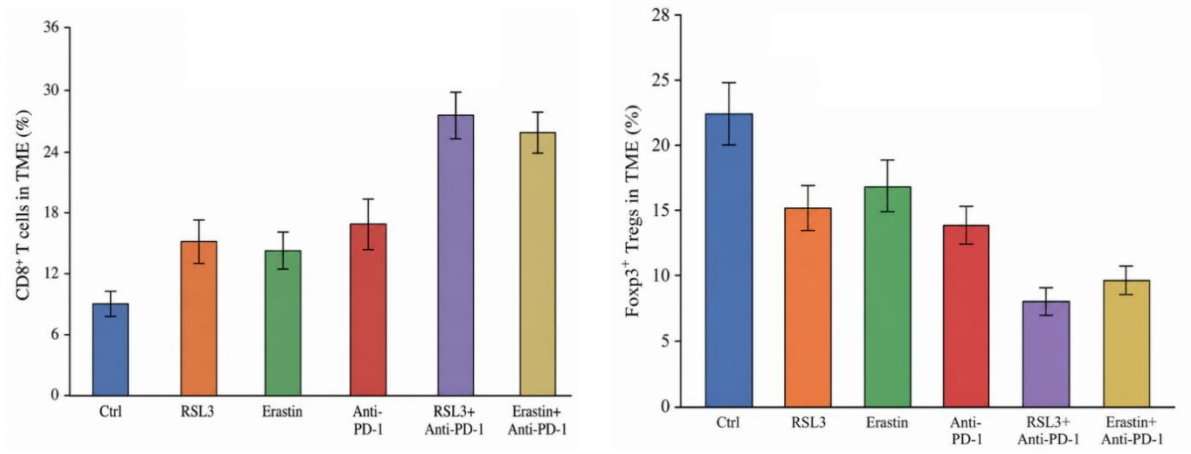

E: Proportion of M2-like macrophages

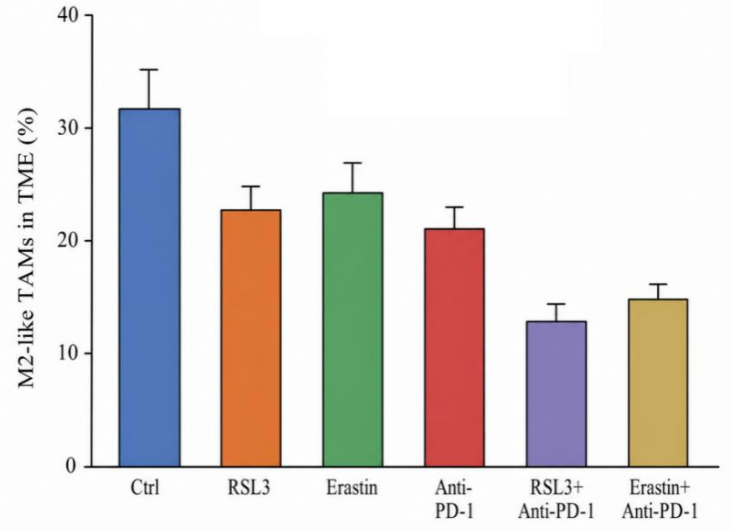

F: Levels of IFN-γ and TGF-β in the TME

Biology and Medical Engineering
WISDOM ACADEMIC https://doi.org/10.63808/bm.v2i1.575 Volume 2 , Issue 1

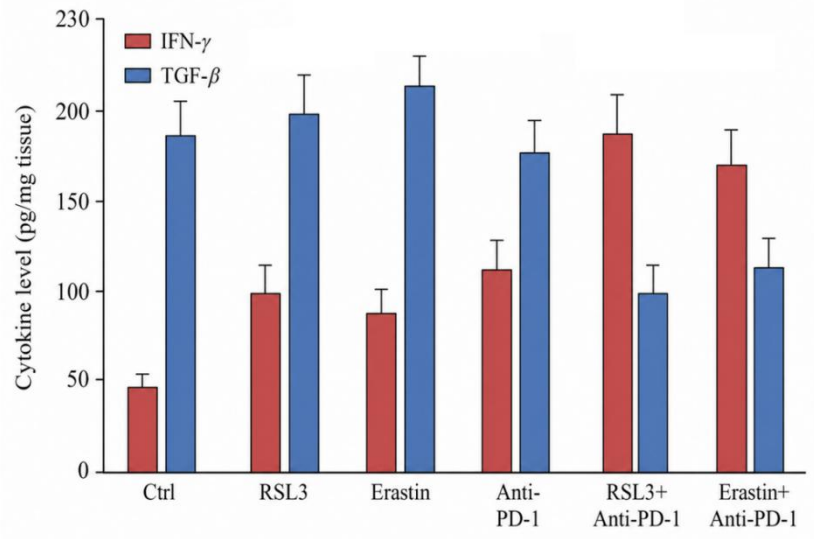

Table 5

In vivo anti-tumor effects and immune remodeling of ferroptosis induction combined with anti-PD-1 therapy

Group	Tumor volume (mm^3, day 21)	Tumor Inhibition Rate (%)	Survival Time (Days)	$CD8^+$ T (%)	Treg (%)	M2 (%)	IFN-γ(pg/mg)	TGF-β(pg/mg)
Control	986.4 ± 112.7	—	28.5 ± 2.1	8.7± 1.2	22.4±2.3	31.7±3.2	45.2 ± 6.1	286.4±28.7
RSL3	612.8 ± 78.5	37.9	36.2 ± 2.8	15.4± 1.8	15.1 ± 1.7	22.5±2.4	98.6± 11.2	198.5±21.3
Erastin	674.3 ± 83.1	31.6	34.7 ± 2.6	13.8± 1.7	16.8 ± 1.9	24.1±2.6	87.3 ± 9.8	215.7±23.6
Anti-PD-1	548.6 ± 69.4	44.4	39.8 ± 3.1	17.2± 2.0	13.9 ± 1.5	20.8±2.2	112.4± 12.7	176.3±18.9
RSL3 + Anti-PD-1	213.5 ± 32.8	78.4	52.6 ± 4.3	28.6± 2.7	8.2 ± 1.0	12.4±1.5	186.5± 18.3	98.6 ± 11.4
Erastin + Anti-PD-1	256.9 ± 37.4	74.0	49.8 ± 4.0	25.9 ± 2.5	9.6 ± 1.1	14.7±1.7	168.9 ± 16.5	112.7±12.8

Table 5A

Tumor growth curves (MC38)

Days	Control	RSL3	Erastin	Anti-PD-1	RSL3 + Anti-PD-1
0	85 ± 9.4	82 ± 9.8	84 ± 10.1	83 ± 10.0	80 ± 11.2
2	155 ± 17.1	128 ± 15.4	136 ± 16.3	118 ± 14.2	96 ± 13.4
4	268 ± 29.5	196 ± 23.5	212 ± 25.4	172 ± 20.6	118 ± 16.5

6	392 ± 43.1	262 ± 31.4	286 ± 34.3	226 ± 27.1	142 ± 19.9
8	528 ± 58.1	336 ± 40.3	372 ± 44.6	288 ± 34.6	158 ± 22.1
10	672 ± 73.9	412 ± 49.4	452 ± 54.2	356 ± 42.7	174 ± 24.4
12	805 ± 88.6	498 ± 59.8	538 ± 64.6	424 ± 50.9	192 ± 26.9
14	912 ± 100.3	562 ± 67.4	606 ± 72.7	488 ± 58.6	204 ± 28.6
16	986 ± 108.5	612 ± 73.4	674 ± 80.9	548 ± 65.8	213 ± 29.8
18	1045 ± 115.0	648 ± 77.8	712 ± 85.4	596 ± 71.5	220 ± 30.8
20	1102 ± 121.2	672 ± 80.6	738 ± 88.6	628 ± 75.4	226 ± 31.6

4.4. The effectiveness of ferroptosis induction combined with anti-PD-1 depends on the GPX4/ACSL4 pathway

To verify the ferroptosis dependence of the combined therapy, we created MC38 cells with GPX4 overexpression and ACSL4 knockout. As shown in Figures 6A-C and Table 6, GPX4 overexpression significantly weakened the tumor-suppressing effect of RSL3 combined with anti-PD-1, with decreases in $CD8^+$ T cell infiltration and survival. ACSL4 knockout similarly reduced the efficacy of the combined treatment. Fer-1 co-treatment also reversed the benefits of the combination therapy.

Figure 6

A: Tumor volume with GPX4/ACSL4 changes

B: $CD8^+$ T cell infiltration with GPX4/ACSL4 changes

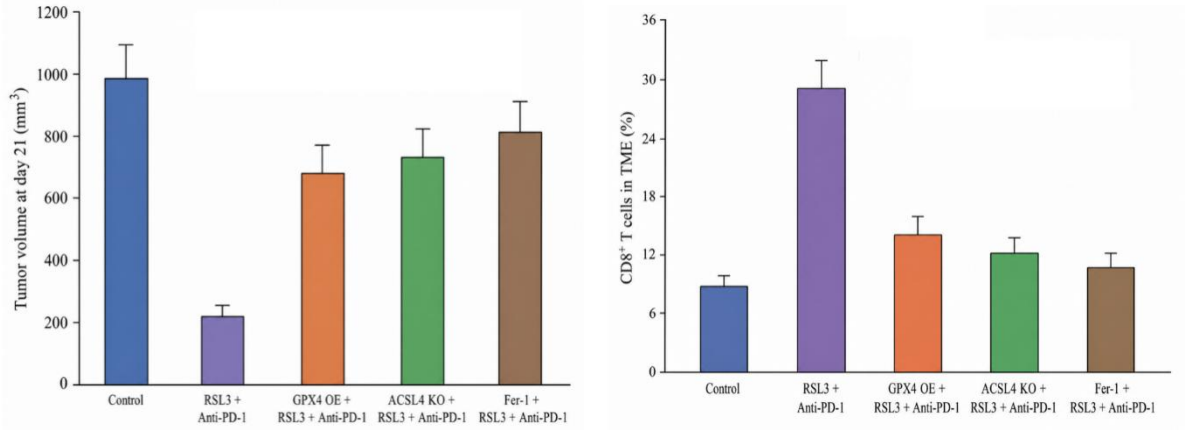

C: Survival with GPX4/ACSL4 changes

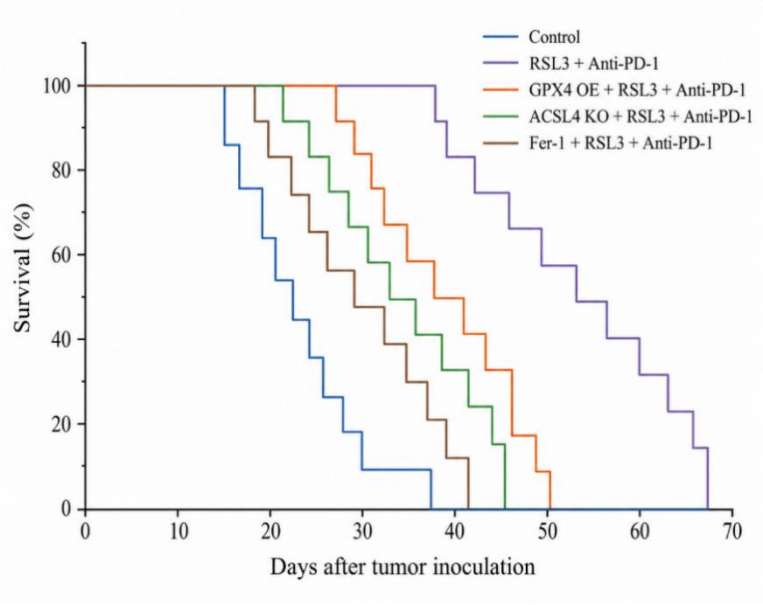

Table 6

The impact of GPX4/ACSL4 on the effectiveness of combined treatment

Model	Tumor volume (mm^3, day 21)	$CD8^+$ T(%)	Survival Time (Days)
Control	978.5 ± 108.3	8.9 ± 1.2	27.8 ± 2.0
RSL3 + Anti-PD-1	221.7 ± 34.6	29.4 ± 2.8	53.2 ± 4.5
GPX4 OE + RSL3 + Anti-PD-1	685.4 ± 79.2	13.5 ± 1.6	35.4 ± 2.9
ACSL4 KO + RSL3 + Anti-PD-1	734.8 ± 85.6	12.1 ± 1.5	33.7 ± 2.7
Fer-1 + RSL3 + Anti-PD-1	812.3 ± 92.4	10.8 ± 1.4	30.5 ± 2.3

4.5. Ferroptosis drives ICD to activate the cGAS-STING pathway and remodel immune metabolism

Mechanism analysis showed that RSL3 treatment significantly increased MDA and 4-HNE levels in tumor tissues, reduced the GSH/GSSG ratio, and activated the cGAS-STING/TBK1/IRF3 pathway (Figures 7A-D, Table 7). After combining with anti-PD-1, p-STING, p-TBK1, and p-IRF3 levels rose further, and IFN-β secretion increased. Overexpressing GPX4 or knocking out ACSL4 both significantly inhibited the activation of these pathways. Single-cell RNA sequencing showed that in the combination treatment group, DC antigen presentation-related genes (H2-Ab1, Cd74, Cd80) and $CD8^+$ T cell effector genes (Ifng, Gzmb, Prf1) were upregulated, while M2-like macrophage pro-tumor genes (Arg1, Mrc1, Tgfb1) were downregulated (Figures 8A-E, Table 8C-E).

Figure 7

A: MDA levels

B: 4-HNE levels

https://doi.org/10.63808/bm.v2i1.575 Volume 2 , Issue 1

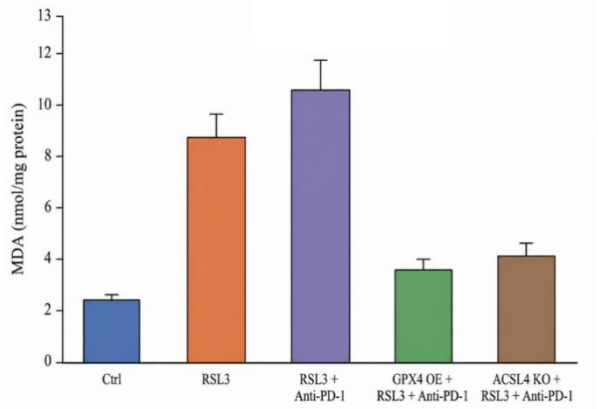

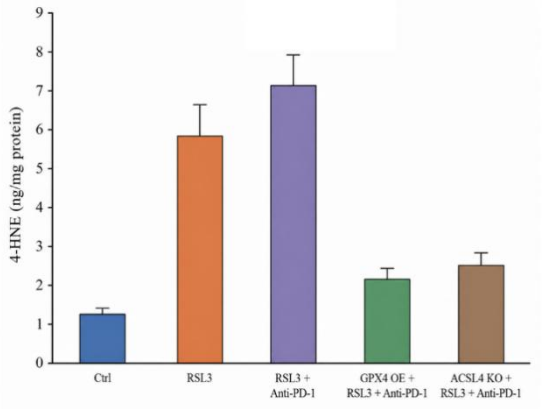

C: GSH/GSSG ratio

D: cGAS-STING pathway activation (phospho-ratio)

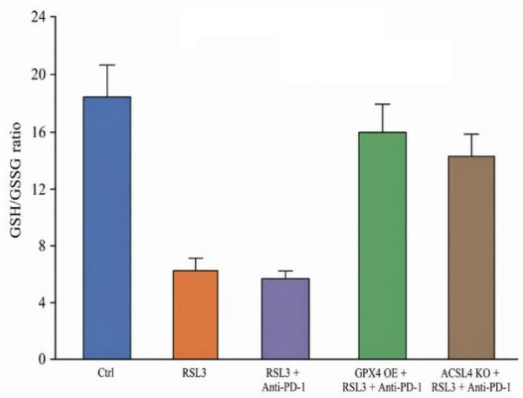

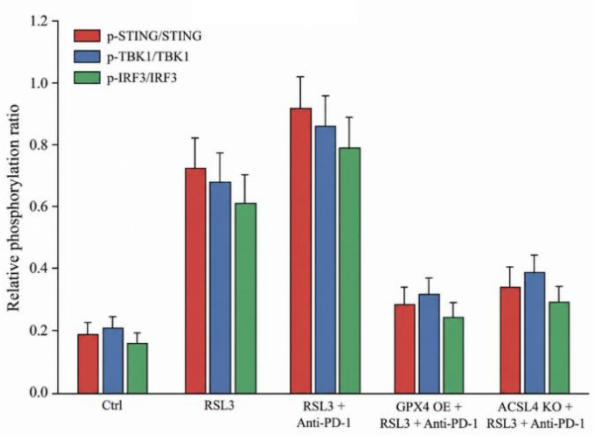

Figure 8

A: UMAP of tumor-infiltrating immune cells

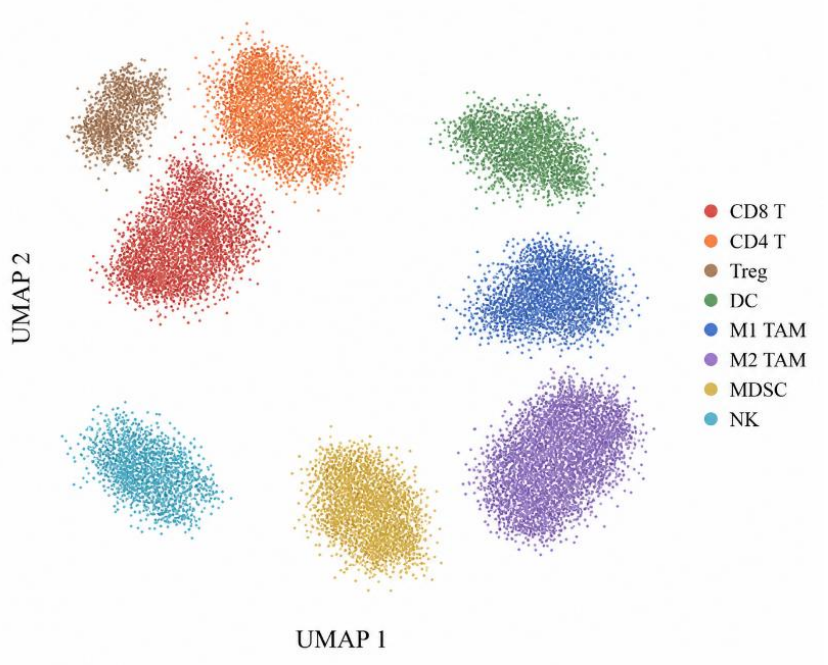

B: UMAP split by treatment group (Control vs RSL3 + Anti-PD-1)

Biology and Medical Engineering
WISDOM ACADEMIC https://doi.org/10.63808/bm.v2i1.575 Volume 2 , Issue 1

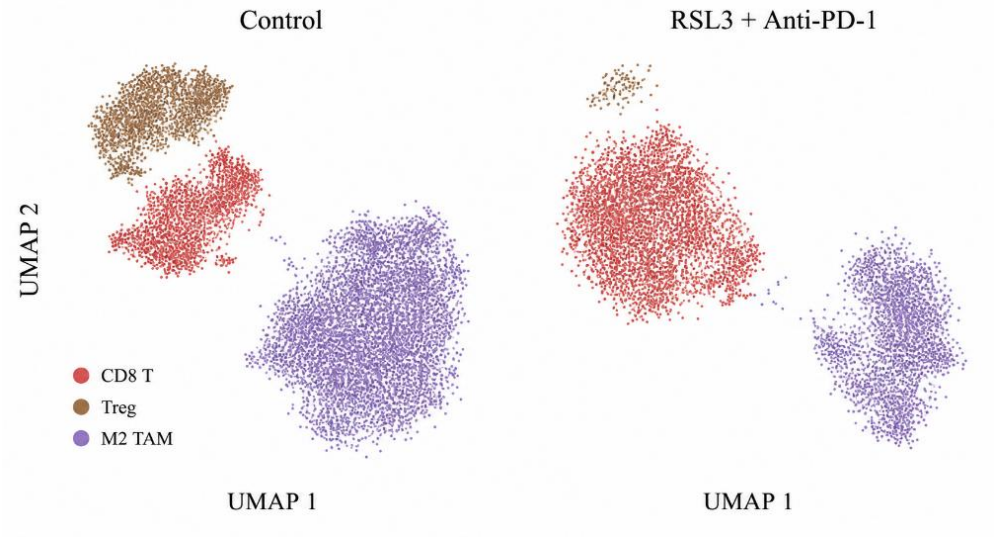

C: Antigen-presentation genes in DCs

D: Effector genes in CD8⁺ T cells

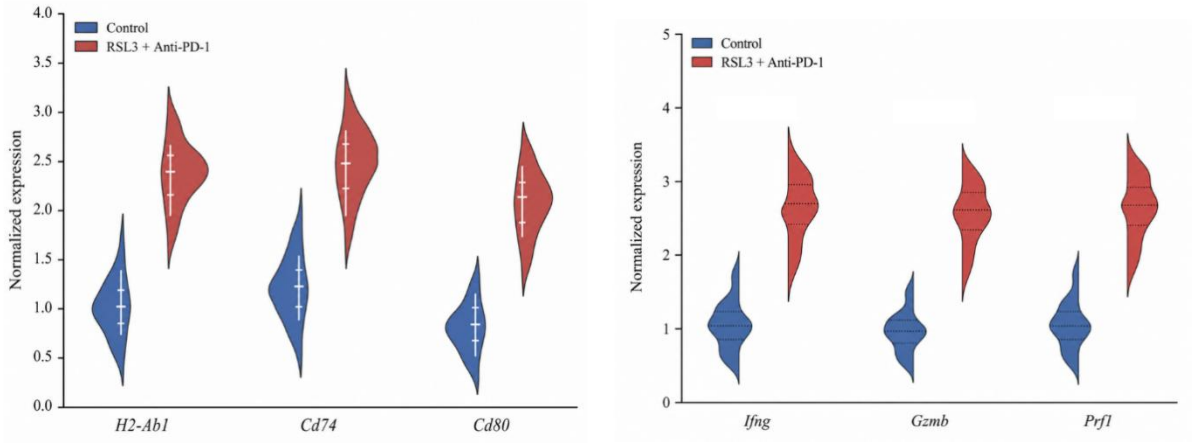

E: Pro-tumor genes in M2-like macrophages

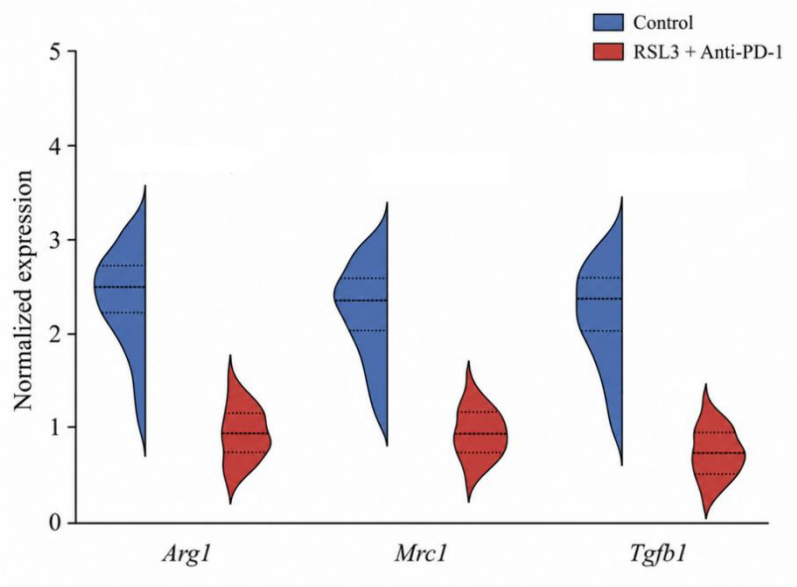

Table 7

Metabolic and signaling pathway indicators related to ferroptosis-driven ICD

Indicator	Control	RSL3	RSL3 + Anti-PD-1	GPX4 OE + RSL3 + Anti-PD-1	ACSL4 KO + RSL3 + Anti-PD-1
MDA(nmol/mg)	2.4 ± 0.3	8.7 ± 0.9	10.5 ± 1.1	3.6 ± 0.4	4.1 ± 0.5
4-HNE(ng/mg)	1.2 ± 0.2	5.8 ± 0.7	7.1 ± 0.8	2.1 ± 0.3	2.5 ± 0.3
GSH/GSSG	18.5 ± 2.1	6.4 ± 0.8	5.8 ± 0.7	15.9 ± 1.8	14.2 ± 1.6
p-STING/STING	0.18 ± 0.03	0.72 ± 0.08	0.91 ± 0.10	0.28 ± 0.04	0.34 ± 0.05
p-TBK1/TBK1	0.21 ± 0.03	0.68 ± 0.07	0.86 ± 0.09	0.31 ± 0.04	0.38 ± 0.05
p-IRF3/IRF3	0.16 ± 0.02	0.61 ± 0.07	0.79 ± 0.08	0.24 ± 0.03	0.29 ± 0.04
IFN-β(pg/mL)	32.5 ± 4.1	145.8 ± 15.2	198.4 ± 20.3	56.7 ± 6.3	68.9 ± 7.5

Table 8C

Antigen-presentation genes in DCs

Gene	Group	Mean ± SD
H2-Ab1	Control	1.0 ± 0.25
H2-Ab1	RSL3 + Anti-PD-1	2.4 ± 0.35
Cd74	Control	1.2 ± 0.28
Cd74	RSL3 + Anti-PD-1	2.6 ± 0.38
Cd80	Control	0.8 ± 0.22
Cd80	RSL3 + Anti-PD-1	2.1 ± 0.30

Table 8D

Effector genes in $CD8^+$ T cells

Gene	Group	Mean ± SD
Ifng	Control	1.0 ± 0.25
Ifng	RSL3 + Anti-PD-1	2.8 ± 0.40
Gzmb	Control	0.9 ± 0.22
Gzmb	RSL3 + Anti-PD-1	2.5 ± 0.36
Prf1	Control	1.1 ± 0.26
Prf1	RSL3 + Anti-PD-1	2.7 ± 0.38

Table 8E

Pro-tumor genes in M2-like macrophages

Gene	Group	Mean ± SD
Arg1	Control	2.6 ± 0.36
Arg1	RSL3 + Anti-PD-1	0.9 ± 0.22
Mrc1	Control	2.4 ± 0.33
Mrc1	RSL3 + Anti-PD-1	1.0 ± 0.24
Tgfb1	Control	2.5 ± 0.35
Tgfb1	RSL3 + Anti-PD-1	0.8 ± 0.20

5. Discussion

This study focused on the core question of whether ferroptosis-driven immunogenic cell death (ICD) can reshape the tumor microenvironment (TME) and boost anti-tumor immunity. We systematically showed that the ferroptosis inducers RSL3 and Erastin can trigger typical ferroptosis in tumor cells, along with upregulation of ICD markers like calreticulin (CRT) surface exposure, HMGB1 release, and ATP secretion. Further research indicated that DAMPs released during ferroptosis can promote dendritic cell (DC) maturation and $CD8^+$ T cell activation, and reshape the TME in vivo, resulting in increased $CD8^+$ T cell infiltration, reduced proportions of Tregs and M2-like macrophages, higher IFN-γ, and lower TGF-β. More importantly, ferroptosis induction showed a significant synergistic effect with anti-PD-1 therapy, dependent on the GPX4/ACSL4-mediated ferroptosis pathway and activation of the cGAS-STING/TBK1/IRF3 signaling. These findings provide experimental evidence for the 'ferroptosis-ICD-immune activation axis' and suggest a new potential strategy for combined cancer immunotherapy.

5.1. New evidence of ferroptosis as an ICD induction method

The core of ICD is that DAMPs released during cell death can turn 'immunologically silent' death into an 'immune-activating' signal. Previous studies mainly focused on classic ICD inducers like anthracyclines, oxaliplatin, and radiotherapy. This study shows that ferroptosis inducers can also trigger typical ICD markers, and that Fer-1 can reverse this process, while the apoptosis inhibitor Z-VAD-FMK has no obvious inhibitory effect. This finding is consistent with Efimova et al., who found that early ferroptotic tumor cell vaccines can induce effective anti-tumor immunity. But our work goes further, analyzing in vitro and in vivo how ferroptosis-driven ICD affects DC maturation, T cell activation, and the immune landscape of the TME, expanding the understanding of the interplay between ferroptosis and ICD at a mechanistic level.

From a mechanistic perspective, during ferroptosis, the accumulation of lipid peroxides, imbalance of GSH/GSSG, and inactivation of GPX4 not only cause damage to cell membranes but

may also activate innate immunity by releasing signaling molecules like oxidized lipids, HMGB1, and ATP. In this study, we observed that after RSL3 treatment, tumor tissues showed significantly increased levels of MDA and 4-HNE, decreased GSH/GSSG ratio, and activation of the cGAS-STING/TBK1/IRF3 pathway, along with increased IFN-β secretion. This suggests that ferroptosis-driven ICD might link innate and adaptive immunity through the cGAS-STING pathway. Compared with the TLR4-dependent mechanism proposed by Apetoh and colleagues, our study adds evidence for a potential role of the cGAS-STING pathway in ferroptosis-ICD, though whether the two pathways work together or show cell type specificity still needs further investigation.

5.2. Comparison with existing anti-tumor immunity research

Wang and others found that IFN-γ from $CD8^+$ T cells can promote tumor cell ferroptosis by downregulating SLC7A11, thereby enhancing the effectiveness of immunotherapy, revealing T cell immunity's regulatory role in ferroptosis. Our study, on the other hand, shows from the opposite direction that inducing ferroptosis can, in turn, promote DC maturation and $CD8^+$ T cell activation, creating a positive feedback loop of 'ferroptosis-ICD-T cell activation.' This finding complements Lang's research on radiotherapy and immunotherapy synergistically suppressing SLC7A11, inducing tumor lipid oxidation and ferroptosis. But our study directly induces ferroptosis with drugs, avoiding the multiple confounding effects of radiotherapy and immunotherapy, and more directly validates the role of ferroptosis itself in remodeling the TME.

Friedmann Angeli and others suggested that ferroptosis sits at the intersection of tumor-acquired drug resistance and immune evasion. Tumor cells can escape ferroptosis through defense systems like GPX4 and SLC7A11, while also shaping an immunosuppressive TME. In this study, we showed through GPX4 overexpression and ACSL4 knockout experiments that the effectiveness of combined therapy depends on the ferroptosis pathway; either GPX4 overexpression or ACSL4 knockout can weaken the tumor-suppressing effect of RSL3 combined with anti-PD-1, reduce $CD8^+$ T cell infiltration, and limit survival benefits. This result not only supports Friedmann Angeli's hypothesis but also provides preclinical evidence for using GPX4/ACSL4 as biomarkers to predict treatment response.

In addition, this study observed at the TME level a decrease in the proportion of Tregs and M2-like macrophages, an increase in IFN-γ, and a decrease in TGF-β, suggesting that ferroptosis-driven ICD might turn a 'cold tumor' into a 'hot tumor.' This is consistent with Krysko and Galluzzi's discussions that ICD can enhance immunogenicity and promote immune cell infiltration. Unlike previous studies that focused on single immune cell subsets, this study combined flow cytometry, multiplex immunohistochemistry, and single-cell RNA sequencing to systematically map the transcriptomic remodeling of multiple immune cell subsets in the TME after ferroptosis induction.

Notably, it revealed upregulation of DC antigen-presenting genes (H2-Ab1, Cd74, Cd80) and $CD8^+$ T cell effector genes (Ifng, Gzmb, Prf1), while M2-like macrophage pro-tumor genes (Arg1, Mrc1, Tgfb1) were downregulated. This provides a more comprehensive evidence chain for the ferroptosis-ICD-immune activation axis.

5.3. Innovation and clinical significance

The innovation of this study mainly lies in four aspects. We proposed and validated a new mechanistic framework called the 'ferroptosis-ICD-immune activation axis,' expanding ferroptosis from merely a form of cell death to a strategy for enhancing immunotherapy. We systematically analyzed how ferroptosis-driven ICD remodels various immune cells in the TME, including DCs, $CD8^+$ T cells, Tregs, and macrophages, going beyond the limitations of previous studies that focused on individual cells or in vitro models. By overexpressing GPX4, knocking out ACSL4, and using Fer-1 interventions, we confirmed the ferroptosis-dependent effect of the combined therapy at both genetic and pharmacological levels. We also revealed the potential bridging role of the cGAS-STING/TBK1/IRF3 pathway in ferroptosis-ICD, providing a mechanistic explanation for combined immune checkpoint inhibition.

From a clinical translation perspective, this study suggests that combining ferroptosis inducers with anti-PD-1 could be a new strategy to overcome resistance to immunotherapy. Especially for immunosuppressive tumors with high GPX4 expression, low ACSL4 expression, or high SLC7A11 expression, inducing ferroptosis might achieve both direct killing and immune activation at the same time. In addition, molecules related to GPX4, ACSL4, MDA, 4-HNE, and the cGAS-STING pathway could serve as markers for predicting efficacy or pharmacodynamics, providing a reference for patient stratification and the design of combination therapies.In recent years, artificial intelligence has been used to predict the effectiveness of tumor immunotherapy and optimize combination strategies by integrating multi-omics data (Liu, 2026b). Explainable spatial AI can analyze tumor-immune interactions, predict immunotherapy outcomes, and identify new targets (Liu et al., 2026d). Multimodal foundation models can predict the immunogenicity of new antigens and the effectiveness of vaccines (Liu et al., 2026e). Therefore, in the future, the ferroptosis-ICD features from this study can be combined with the above computational framework to build a multimodal prediction model, in order to identify patients who are most likely to benefit from ferroptosis-induced combined immune checkpoint blockade.

5.4. Limitations and future directions

Although this study provides relatively systematic evidence, there are still several limitations. The research is mainly based on MC38 and B16-F10 mouse tumor models, which cover colon cancer and melanoma, but human tumors are more heterogeneous. The efficacy and immune effects of

ferroptosis inducers in different cancer types still need to be verified in humanized mice, organoids, or clinical samples. While RSL3 and Erastin are widely used in ferroptosis studies, they may have off-target effects; although experiments with Fer-1, GPX4 overexpression, and ACSL4 knockout support ferroptosis dependency, other forms of cell death or non-ferroptotic pathways cannot be completely ruled out. This study has not yet distinguished the relative contribution of tumor cell ferroptosis versus immune cell ferroptosis to TME remodeling; whether ferroptosis inducers affect the ferroptosis sensitivity of T cells, DCs, or macrophages themselves still needs to be clarified through conditional gene knockout or cell-specific interventions. The causal role of the cGAS-STING pathway is mainly based on pharmacology and expression correlation analysis, and future validation should involve Sting1 knockout, cGAS knockout, or combined experiments with STING agonists/inhibitors. The in vivo toxicity, pharmacokinetics, and long-term safety of ferroptosis inducers are still unclear, especially the risk of immune-related adverse events when combined with anti-PD-1 therapy, which needs systematic evaluation. Single-cell RNA sequencing only included limited time points and treatment groups, possibly missing the dynamic immune remodeling processes; integrating spatial transcriptomics and multiplex imaging will help to more accurately dissect the spatiotemporal effects of ferroptosis-ICD.

Future research could go in the following directions: developing tumor-targeted ferroptosis inducers or nano-delivery systems to improve tumor selectivity and reduce systemic toxicity; exploring the best combination strategies of ferroptosis induction with radiotherapy, chemotherapy, other immune checkpoint inhibitors, adoptive cell therapy, gut microbiota-primed immunity, and in vivo CAR-T and other novel immunotherapies (Liu et al., 2026f; Liu et al., 2026g). Using humanized mice, patient-derived organoids, and clinical cohorts to validate the value of the GPX4/ACSL4/cGAS-STING axis as a biomarker; combining spatial multi-omics and metabolic flux analysis to decipher the spatiotemporal dynamics of DAMPs release, antigen presentation, and T cell activation during ferroptosis-ICD; and assessing the long-term effects of ferroptosis induction on immune cell function and immune memory.

6. Conclusion

This study systematically shows that the ferroptosis inducers RSL3 and Erastin can trigger ferroptosis in tumor cells along with the release of immunogenic cell death (ICD) markers, including calreticulin exposure on the membrane, HMGB1 release, and ATP secretion. Ferroptosis-driven ICD can promote dendritic cell maturation and $CD8^+$ T cell activation, and remodel the tumor microenvironment in vivo, leading to increased $CD8^+$ T cell infiltration, reduced Tregs and M2-like macrophages, higher IFN-γ, and lower TGF-β. Importantly, inducing ferroptosis works synergistically with anti-PD-1 therapy for a strong anti-tumor effect, which depends on the GPX4/ACSL4-mediated

ferroptosis pathway and activation of the cGAS-STING/TBK1/IRF3 signaling. These findings support the 'ferroptosis-ICD-immune activation axis' as a new framework for tumor immunotherapy and provide a preclinical basis for combining ferroptosis induction with immune checkpoint blockade.

Although this study is still limited by factors such as the types of models used, off-target effects of drugs, and the contribution of immune cell-specific ferroptosis, future research could further validate the safety and effectiveness of this strategy in humanized mice, patient-derived organoids, and clinical cohorts. At the same time, tumor-targeted ferroptosis inducers or nano-delivery systems should be developed, and combination strategies with radiotherapy, chemotherapy, and other immunotherapies should be optimized. It's also important to systematically evaluate the value of GPX4, ACSL4, MDA, 4-HNE, and cGAS-STING pathway-related molecules as biomarkers for predicting treatment efficacy. Combining spatial multi-omics, metabolic flux analysis, and immune memory studies will help deepen our understanding of the spatiotemporal dynamics of ferroptosis-ICD and its long-term immune effects, promoting the clinical translation of this strategy.

Acknowledgments

Not applicable.

Author contributions

Conceptualization, Gang Liu; methodology, Jia Wang; validation, Alena Mikalaeuna Vasiukevich; formal analysis, Biao Feng and Liqiang An; investigation, Jia Wang and Biao Feng; resources, Gang Liu and Liqiang An; data curation, Alena Mikalaeuna Vasiukevich; writing—original draft preparation, Jia Wang; writing—review and editing, Gang Liu and Alena Mikalaeuna Vasiukevich; visualization, Biao Feng; supervision, Gang Liu; project administration, Liqiang An. All authors have read and agreed to the published version of the manuscript.

Funding

Not applicable.

Data availability

Not applicable.

Declarations

Conflict of interest

The authors declare that there is no conflict of interest.

Ethics approval

Not applicable.

Consent to participate

Not applicable.

Consent for publication

All authors have given their consent.

Additional information

Received: 13 November 2026

Accepted: 13 November 2026

Published online:

Publisher's Note

Wisdom Academic Press Ltd. remains neutral with regard to jurisdictional claims in published maps and institutional affiliations.

References

[1] Apetoh, L., Ghiringhelli, F., Tesniere, A., et al. (2007). Toll-like receptor 4-dependent contribution of the immune system to anticancer chemotherapy and radiotherapy. *Nat Med, 13*(9), 1050-1059. https://doi.org/10.1038/nm1622

[2] Dixon, S. J., Lemberg, K. M., Lamprecht, M. R., et al. (2012). Ferroptosis: An iron-dependent form of nonapoptotic cell death. *Cell, 149*(5), 1060-1072. https://doi.org/10.1016/j.cell.2012.03.042

[3] Doll, S., Proneth, B., Tyurina, Y. Y., et al. (2017). ACSL4 dictates ferroptosis sensitivity by shaping cellular lipid composition. *Nat Chem Biol, 13*(1), 91-98. https://doi.org/10.1038/nchembio.2239

[4] Efimova, I., Catanzaro, E., Van der Meeren, L., et al. (2020). Vaccination with early ferroptotic cancer cells induces efficient antitumor immunity. *J Immunother Cancer, 8*(2), e001369. https://doi.org/10.1136/jitc-2020-001369

[5] Friedmann Angeli, J. P., Krysko, D. V., & Conrad, M. (2019). Ferroptosis at the crossroads of cancer-acquired drug resistance and immune evasion. *Nat Rev Cancer, 19*(7), 405-414. https://doi.org/10.1038/s41568-019-0149-1

[6] Galluzzi, L., Buqué, A., Kepp, O., Zitvogel, L., & Kroemer, G. (2017). Immunogenic cell death in cancer and infectious disease. *Nat Rev Immunol, 17*(2), 97-111. https://doi.org/10.1038/nri.2016.107

[7] Kepp, O., Senovilla, L., Vitale, I., et al. (2014). Consensus guidelines for the detection of immunogenic cell death. *Oncoimmunology, 3*(9), e955691. https://doi.org/10.4161/21624011.2014.955691

[8] Krysko, D. V., Garg, A. D., Kaczmarek, A., et al. (2012). Immunogenic cell death and DAMPs in cancer therapy. *Nat Rev Cancer, 12*(12), 860-875. https://doi.org/10.1038/nrc3380

[9] Lang, X., Green, M. D., Wang, W., et al. (2019). Radiotherapy and immunotherapy promote tumoral lipid oxidation and ferroptosis via synergistic repression of SLC7A11. *Cancer Discov, 9*(12), 1673-1685. https://doi.org/10.1158/2159-8290.CD-19-0338

[10] Lei, G., Zhuang, L., & Gan, B. (2022). Targeting ferroptosis as a vulnerability in cancer. *Nat Rev Cancer, 22*(7), 381-396. https://doi.org/10.1038/s41568-022-00459-0

[11] Liu, G. (2026a). Tumor microenvironment: composition, dynamic evolution, and its significance in cancer treatment. *Journal of Cancer Insights, 1*(1), 6. https://doi.org/10.66128/jci202601.1

[12] Liu, G. (2026b). The application of artificial intelligence in tumor immunotherapy: Integrating multi-omics data to achieve efficacy prediction and combination strategies. *Applied Artificial Intelligence Research, 2*(2). https://doi.org/10.65455/q72yq328

[13] Liu, G., & Vasiukevich, A. M. (2026g). CD5-targeted LNP-mRNA generates CD19 CAR-T cells in the body to achieve lupus remission without clearing lymph nodes. *Journal of New Engineering Industry in South Taihu, 1*(1), 24-38. https://doi.org/10.68249/jstnei.2026.0006

[14] Liu, G., Wang, J., & An, L. (2026b). Mitochondrial DNA sensing reshapes the tumor immune microenvironment via cooperative cGAS-STING activation and ferroptosis. *Global Health Care, 2*(1). https://doi.org/10.63808/ghc.v2i1.524

[15] Liu, G., Wang, J., & An, L. (2026c). CRISPR screen and single-cell multi-omics identify a novel immune checkpoint on tumor-infiltrating regulatory T cells. *Injury and Rehabilitation Care, 2*(1). https://doi.org/10.63808/irc.v2i1.525

[16] Liu, G., Wang, J., & An, L. (2026f). Gut microbiota-derived butyrate induces trained immunity in intestinal macrophages to potentiate antitumor immunity. *Biology and Medical Engineering, 2*(1). https://doi.org/10.63808/bm.v2i1.523

[17] Liu, G., Wang, J., & Zhu, J. (2026d). Explainable spatial AI analyzes tumor-immune interactions to predict immunotherapy outcomes and identify new targets. *Intelligent & Human Futures, 2*(3). https://doi.org/10.63808/ihf.v2i3.510

[18] Liu, G., Wang, J., & Zhu, J. (2026e). Using multimodal foundational models to predict neoantigen immunogenicity and vaccine effectiveness across different tumor types. *Global Health Care, 2*(3). https://doi.org/10.63808/ghc.v2i3.498

[19] Liu, G., Wang, J., Vasiukevich, A. M., Feng, B., An, L. (2026a). Targeting mitochondrial metabolic reprogramming: Reversing $CD8^+$ T cell exhaustion and improving cancer immunotherapy response. *Biology and Medical Engineering, 2*(1). https://doi.org/10.63808/bm.v2i1.531

[20] Obeid, M., Tesniere, A., Ghiringhelli, F., et al. (2007). Calreticulin exposure dictates the immunogenicity of cancer cell death. *Nat Med, 13*(1), 54-61. https://doi.org/10.1038/nm1523

[21] Stockwell, B. R., Friedmann Angeli, J. P., Bayir, H., et al. (2017). Ferroptosis: A regulated cell death nexus linking metabolism, redox biology, and disease. *Cell, 171*(2), 273-285. https://doi.org/10.1016/j.cell.2017.09.021

[22] Tang, D., Chen, X., Kang, R., & Kroemer, G. (2021). Ferroptosis: Molecular mechanisms and health implications. *Cell Res, 31*(2), 107-125. https://doi.org/10.1038/s41422-020-00441-1

[23] Wang, W., Green, M., Choi, J. E., et al. (2019). CD8+ T cells regulate tumour ferroptosis during cancer immunotherapy. *Nature, 569*(7755), 270-274. https://doi.org/10.1038/s41586-019-1170-y

[24] Yang, W. S., SriRamaratnam, R., Welsch, M. E., et al. (2014). Regulation of ferroptotic cancer cell death by GPX4. *Cell, 156*(1-2), 317-331. https://doi.org/10.1016/j.cell.2013.12.010